MEDICAL SCIENCE MONITOR

CLINICAL RESEARCH

e-ISSN 1643-3750
© Med Sci Monit, 2017; 23: 4533-4540
DOI: 10.12659/MSM.903974

Received: 2017.02.22
Accepted: 2017.03.20
Published: 2017.09.21

Positron Emission Tomographic Imaging Elucidates the Complex Relationship Between Glucose Uptake and Tissue Blood Flow Mechanism in Squamous Cell Oral Cancer Patients

Authors' Contribution:
Study Design A
Data Collection B
Statistical Analysis C
Data Interpretation D
Manuscript Preparation E
Literature Search F
Funds Collection G

ABC Ping Xu
DF Yan Li
AE Shuyong Yang
CF Mingzhe Li
E Chenjun Li

Department of Stomatology, Chengdu Military General Hospital, Chengdu, Sichuan, P.R. China

Corresponding Author: Chenjun Li, e-mail: luciana.rymer8678@hotmail.com
Source of support: Departmental sources

Background: Through the clinical use of positron emission tomography, we aimed to elucidate the complex relationship between glucose uptake and squamous cell oral cancer (ScOC) growth, along with its mechanism with respect to tissue blood flow (tBF).

Material/Methods: We retrospectively reviewed a total of 69 newly diagnosed ScOC patients by Fluorine-18 fluorodeoxyglucose (18F-FDG) positron emission tomography (PET). Maximum and mean standard uptake values (SUV$\uparrow$ and $\overline{\text{SUV}}$) were recorded to assess glucose uptake. Multi-shot spin-echo echo-planar imaging-based pseudo-continuous arterial spin labeling (pcASL) technique at 3.0 T MRI was used to obtain tBF values in ScOC (tBF-ScOC). Patients were divided according to T-stage and location. Pearson's correlation coefficients were calculated between both SUV and tBF-ScOC for significant correlations.

Results: Forty-one (59.4%) patients had oropharynx and the other 28 (40.6%) patients had laryngopharynx. Significant positive correlations were detected between SUV$\uparrow$, $\overline{\text{SUV}}$, tBF-ScOC and non-advanced T-stage (T_{1a}, T_{1b}, T_2 and T_3), while a negative correlation was observed in the advanced T-stage (T_{4a} and T_{4b}).

Conclusions: Using PET imaging, we established the relationship between glucose uptake and ScOC growth on the basis of the division of T-stage and tumor location of ScOC, thereby elucidating the underlying mechanism. Our findings provide insights important to the diagnosis, treatment, and care of ScOC patients.

MeSH Keywords: Carcinoma, Squamous Cell • Oropharynx • Positron-Emission Tomography

Full-text PDF: https://www.medscimonit.com/abstract/index/idArt/903974

Indexed in: [Current Contents/Clinical Medicine] [SCI Expanded] [ISI Alerting System] [ISI Journals Master List] [Index Medicus/MEDLINE] [EMBASE/Excerpta Medica] [Chemical Abstracts/CAS] [Index Copernicus]

Background

Positron emission tomography (PET) is a technique based on positron emission imaging; it is broadly utilized in early detection and is followed by treatment of squamous cell oral cancer (ScOC) and other diseases [1–3]. This happens only when biomolecules are labeled with a positron-emitting isotope and then those biomolecules are incorporated prior to executing image-based studies. Fluorine-18 has a positron-emitting character and favorable half-life of <110 min; therefore, it has been widely used in radiolabeling of biomolecules for PET. Specifically, fluorine-18 fluorodeoxyglucose (^{18}F-FDG), an analogue of glucose, has been recently used for this purpose because, via the Warburg effect, it is taken up by tumor cells, affecting the glycolytic rate. PET technique using ^{18}F-FDG may be used to assess the extent of malignancy in ScOC [4–7].

Oesophageal cancer is the 8th most common cancer worldwide [8]. More than half of Chinese cancer patients have ScOC as the dominant disease [9]. Several studies have demonstrated that 2 biological factors – glucose uptake and tissue blood flow in ScOC (tBF-ScOC) – can assist in the diagnosis and treatment of ScOC [10–12]. Since fused ^{18}F-FDG with PET interprets the tumor metabolic rate of glucose, it directly measures the tumor aggressiveness simply by determining the tumor's FDG uptake, thus enhancing the accuracy of diagnosis [11,12]. For this purpose, a semi-quantitative parameter known as maximum standard uptake value (SUV$\uparrow$) has been used previously in ^{18}F-FDG PET for prognosis and treatment guidance in various tumors [13–15]. Another tumor characteristic – tumor neo-angiogenesis – is reflected by tBF-ScOC and has played an essential role in pre-treatment assessment of the need for chemoradiotherapy in these patients [16,17]. Recently, an advanced technique – pseudo-continuous arterial spin labeling (pcASL) – has been introduced and used to measure tissue blood flow in specific diseases [18,19], such as in investigating the role of cerebral blood flow in survival rate of patients with recurrent high-grade gliomas [20]. Interestingly, the association between several specific microRNAs and ScOC has been reported [21–23].

There have been few reports on the relationship between glucose uptake and ScOC growth with respect to tBF [24–27]; therefore, the mechanism underlying its behavior in ScOC is unclear and needs to be investigated. Due to the limited available information and the utility of ^{18}F-FDG PET and pcASL, performed the present study, which is the first to elucidate the complex relationship of glucose uptake with ScOC growth, along with its tBF mechanism, in these patients.

Table 1. Clinicopathologic characteristics (n=69).

Characteristic	No. of patients (%)	
Age (yr)/median (range)	62.6/26–79	
Gender		
Male	49	(71)
Female	20	(39)
Histology		
Well	17	(25)
Moderate	38	(55)
Poor	14	(20)
Location		
Oropharynx (Op)	42	(61)
Larygopharynx (Lp)	27	(39)
Pathological T stage	For Op	For Lp
T_{1a}	1	1
T_{1b}	2	1
T_{2}	9	6
T_{3}	9	5
T_{4a}	14	11
T_{4b}	7	3

Material and Methods

Patients

Our study was approved by the Institutional Review Board of our hospital. The requirement of written informed consent from the enrolled subjects (patients) was waived because of the retrospective nature of our study. The exclusion criteria included: (a) absence of first diagnosis of ScOC in the patients; (b) lack of performing both MR and PET/CT scanning before any treatment; (c) histology other than ScOC; (d) absence of the scan interval between MR and PET/CT was less than 20 days, and (e) chemotherapy or chemoradiation. The latest preoperative procedure was used as the inclusion criteria based upon clinicopathologic characteristics of the subjects (Table 1).

^{18}F-FDG PET imaging

An advanced PET-CT scanner (Discovery IQ, GE Healthcare, Waukesha, WI) was used to obtain ^{18}F-FDG PET-CT scans. After fasting for >6 h, all patients received an intravenous injection

Indexed in: [Current Contents/Clinical Medicine] [SCI Expanded] [ISI Alerting System] [ISI Journals Master List] [Index Medicus/MEDLINE] [EMBASE/Excerpta Medica] [Chemical Abstracts/CAS] [Index Copernicus]

of 370 MBq ±10% (10 mCi) of ^{18}F-FDG after initial preparation and then waited 60 min post-injection. After this initial preparation, patients were subjected to their PET examination, having an energy window of range of 400–600 keV. A 3D emission scanning was then performed for 3 min for each bed position by keeping the respective axial and trans-axial field of views at 22.2 cm and 60.7 cm. We acquired CT-derived attenuation-corrected images without using any contrast medium. As per previously reported methods [27,28] these images were reconstructed using integrated iterative method followed by conducting a system matrix derived from point source measurements. For semi-quantitative analysis of ^{18}F-FDG uptake, both the SUVs (SUV$^{\uparrow}$ and $\overline{\text{SUV}}$) were assessed. For this purpose, calculations from attenuation-corrected images, the amount of injected ^{18}F-FDG, the body weight of each patient, and the cross-calibration factors for ^{18}F-FDG PET were conducted.

pcASL Imaging acquisition

We used multi-shot spin-echo echo-planar imaging to obtain controlled and labeled images during the performance of the acquisition of pcASL images. As standard protocol, we used T_2-weighted images (T_2WI) as the reference and placed the labeling slab just under the branching of the external and internal carotid arteries. The pCASL imaging parameters were: 1.7 s/1.4 s/3626 ms/15 ms/90°/240×240 mm/2/80×80/18/5 mm/2/300 s (labeling pulse duration/post-labeling delay/no flow crushing gradient, TR/no flow crushing gradient, TE/flip angle/field-of-view/number of shots/matrix/number of slices/slice thickness/parallel imaging acceleration factor/scan time). Similarly, other conventional MR images were obtained for axial and coronal T_2WI map parameter with a turbo spin-echo (TSE) sequence and axial T_1-weighted images (T_1WI) with a gradient-echo sequence using the following parameters: 4.6 s/75 ms/8/250×250 mm/256×256/30%/5 mm/130 s (TR/TE/TSE/field-of-view/matrix/inter-slice gapping/slice thickness/scan time); and 4.6 s/15 ms/7°/250×250 mm/256×256/30%/10 mm/8 s (TR/TE/constant flip angle/field-of-view/matrix/inter-slice gapping/slice thickness (single-slice acquisition)/scan time), respectively. The coil was attached tightly to the head to stop any possible movement during the scan. In addition to this, the patients were also instructed not to make any voluntary motion, including moving, swallowing, or opening their mouths during the pCASL scan.

pcASL Image quality assessment

We compared the pixel values of controlled and labeled images. We obtained several negative-value pixels when there appeared to be misregistration in both the controlled and labeled images caused by vigorous motion during the scan. We neglected negative-valued pixels that exceeded 25% of all pixels in the tumor region of interest.

Quantification of tBF-ScOC by pcASL

As per previously reported works [29–31], we quantified the tBF-ScOC by pcASL (ψ) by calculating it from the signal difference (ΔS), after subtraction of the labeled image from the controlled image, as per the following equation:

$$\psi = \frac{\varepsilon\varphi e^{\tau\varphi}\Delta S}{2(1 - e^{-\sigma\varphi})E\delta} \quad (1)$$

where ε is the blood/tumor-tissue water partition coefficient (1.0 g/mL), φ is the longitudinal relaxation rate of blood (0.67/s), τ is the post-labeling delay time (1.28 s), σ is the labeling time (1.65 s), E is the equilibrium magnetization of the cancerous tissue, and δ is the labeling efficiency (0.85). We obtained φ by the T_1 map and estimated the value of E from the intensity of the controlled image signal. We created tBF-ScOC maps pixel-by-pixel by using Equation (1) and then used MATLAB (MathWorks, Natick, MA) to calculate the tBF-ScOC values.

Data analysis

We estimated the uptake in the tumor using the maximum and mean standard uptake values (SUV$^{\uparrow}$ and $\overline{\text{SUV}}$) in order to quantify the FDG uptake in the primary tumor. For this purpose, we used an isocontour threshold method to determine the automated region of interest (ROI) for both SUVs. As per reported work [31] we set threshold SUV value at 2.5 for the tumor ROI delineation to exclude nearly normal tissue uptake or central necrosis. Within the tumor ROI, the highest SUV value was taken as SUV$^{\uparrow}$ while the average of the SUV values was taken as $\overline{\text{SUV}}$. In a few cases in which the tumor extended to 2 or more slices, we defined SUV$^{\uparrow}$ as the highest SUV value in all slices and defined as the mean SUV value of all pixels in all ROIs of the cancer.

For calculating tBF-ScOC values we used Image J software (National Institutes of Health, Bethesda, MD, USA) to perform ROI delineation on the axial T_2WI with a polygonal ROI, followed by copying the ROI onto a tBF-ScOC map and also included the soft-tissue mass in the ROI obtained from the T_2WI imaging findings. We excluded the normal or inflammatory tumor in the ROI. T_1WI was used to guide the determination of ROI. During quantification of tBF-ScOC, we excluded the outlined area of the vessel signal void on the T_2WI to avoid vascular artifacts in the ROI. Additionally, we also excluded any strong high-signal area with T_2WI which indicated the presence of necrosis. We took the mean of the tBF-ScOC values in the outlined ROI as our anticipated tBF-ScOC value for each patient. Cases in which the tumor reached up to ≥2 slices, we took the anticipated tBF-ScOC value as the mean tBF-ScOC value of all pixels in all ROIs of the cancerous tissue.

Indexed in: [Current Contents/Clinical Medicine] [SCI Expanded] [ISI Alerting System] [ISI Journals Master List] [Index Medicus/MEDLINE] [EMBASE/Excerpta Medica] [Chemical Abstracts/CAS] [Index Copernicus]

Table 2. Standard uptake value and tissue blood flow in squamous cell oral cancer patients (n=69).

Category/combination	SUV↑ (mean, SD)	$\overline{SUV}$ (mean, SD)	tBF-ScOC* (mean, SD)
(a) Division with respect to T-stage			
NAS: $T_{1a}/T_{1b}/T_2/T_3$ (n=34)	21.8, 5.2	11.1, 2.2	135.4, 40.6
AS: T_{4a}/T_{4b} (n=35)	23.4, 6.3	11.3, 2.8	119.8, 38.4
(b) Division with respect to location			
Op (n=42)	20.6, 5.5	10.2, 4.3	118.3, 43.6
Lp (n=27)	21.2, 6.9	10.7, 4.0	117.5, 41.1
(c) All subjects (patients; n=69)	24.3, 7.4	11.9, 2.3	118.7, 40.3
Combinations			
(1) NAS ($T_{1a}/T_{1b}/T_2/T_3$) category with Op (n=21)	23.6, 6.7	10.8, 2.9	121.3, 39.5
(2) NAS ($T_{1a}/T_{1b}/T_2/T_3$) category with Lp (n=13)	23.2, 6.1	10.9, 3.1	123.4, 38.7
(3) AS (T_{4a}/T_{4b}) category with Op (n=21)	24.9, 7.2	11.5, 3.4	124.4, 41.4
(4) AS (T_{4a}/T_{4b}) category with Lp (n=14)	24.5, 7.7	11.5, 2.2	125.2, 42.6

SUV↑ – maximum standard uptake values; $\overline{SUV}$ – mean standard uptake values; tBF-ScOC – tissue blood flow in ScOC; * ml/100 g/min; SD – standard deviation; NAS – non-advanced stage; AS – advanced stage; Op – oropharynx locality category; Lp – larygopharynx locality category.

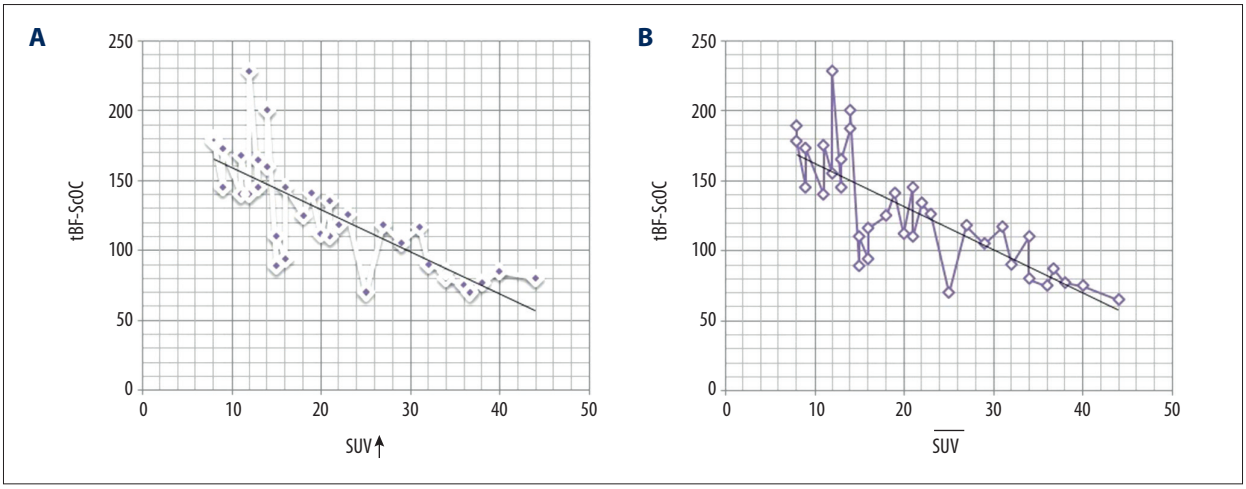

Figure 1. Scatter plot (with straight lines) of the SUV (SUV↑$\overline{SUV}$) and tBF-ScOC values in all patients with advanced T-stage (T_{4a} and T_{4b}) (n=35). There were significant negative correlations (in terms of Pearson's correlation coefficient (r)): (**A**) between SUV↑ and tBF-ScOC values (–0.70 (p<0.05)); and (**B**) between $\overline{SUV}$ and tBF-ScOC values (-0.73 (p<0.05)).

Statistical analysis

On the basis of Pearson's correlation coefficient (r), defined as: <0.2/0.2–0.4/0.41–0.6/0.61–0.8/≥0.81 (poor/weak/moderate/good/excellent correlation), the correlations between the tBF-ScOC values and SUV values (SUV↑ and $\overline{SUV}$) were analyzed. We divided the correlation analysis between SUVs and tBF-ScOCs into 3 categories for convenience as: (a) each patient category divided by tumor T-stage (non-advanced stage: $T_{1a}/T_{1b}/T_2/T_3$ and advanced stage: T_{4a}/T_{4b}); (b) each patient category divided by tumor location (oropharynx and laryngopharynx localities); and (c) all patients category. The level of significance was set at p<0.05. These categories were further divided into 4 combinations for correlation analysis as: (1) non-advanced stage ($T_{1a}/T_{1b}/T_2/T_3$) category with oropharynx locality category; (2) non-advanced stage ($T_{1a}/T_{1b}/T_2/T_3$) category with

Indexed in: [Current Contents/Clinical Medicine] [SCI Expanded] [ISI Alerting System] [ISI Journals Master List] [Index Medicus/MEDLINE] [EMBASE/Excerpta Medica] [Chemical Abstracts/CAS] [Index Copernicus]

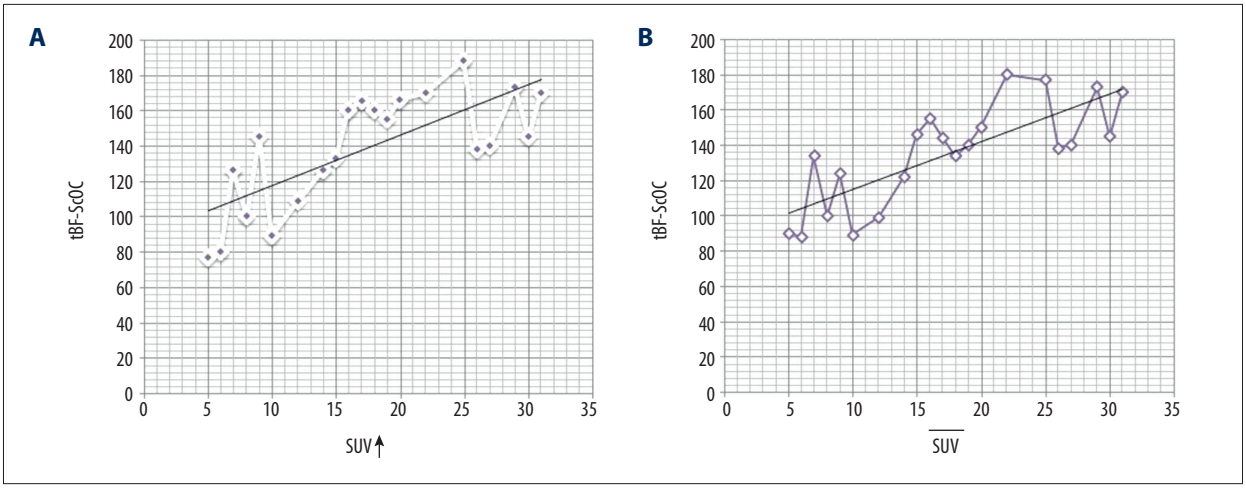

Figure 2. Scatter plot (with straight lines) of the SUV (SUV↑/$\overline{SUV}$) and tBF-ScOC values in the combination of oropharynx locality category patients with non-advanced T-stage (T_{1a}, T_{1b}, T_2 and T_3) (n=21). There were significant positive correlations (in terms of Pearson's correlation coefficient (r)): (**A**) between SUV↑ and tBF-ScOC values (0.75 ($p<0.05$)); and (**B**) between $\overline{SUV}$ and tBF-ScOC values (0.77 ($p<0.05$)).

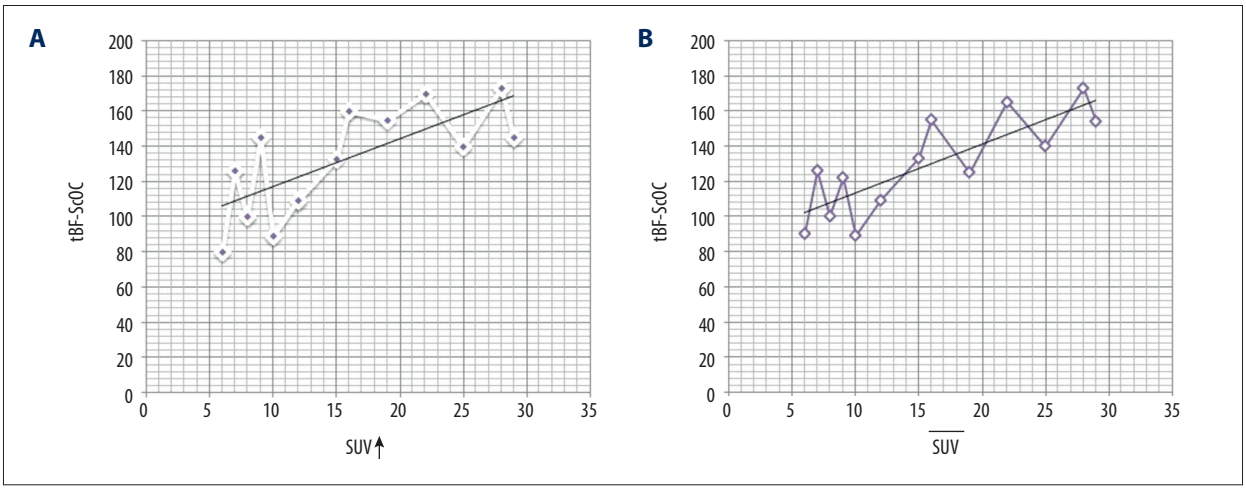

Figure 3. Scatter plot (with straight lines) of the SUV (SUV↑/$\overline{SUV}$) and tBF-ScOC values in the combination of laryngopharynx locality category patients with non-advanced T-stage (T_{1a}, T_{1b}, T_2, and T_3) (n=13). There were significant positive correlations (in terms of Pearson's correlation coefficient (r)): (**A**) between SUV↑ and tBF-ScOC values (0.71 ($p<0.05$)); and (**B**) between $\overline{SUV}$ and tBF-ScOC values (0.73 ($p<0.05$)).

laryngopharynx locality category; (3) advanced stage (T_{4a}/T_{4b}) category with oropharynx locality category; and (4) advanced stage (T_{4a}/T_{4b}) category with laryngopharynx locality category.

Results

Table 2 summarizes the average SUV↑, $\overline{SUV}$ and tBF-ScOC values in ScOC values in each patient category. No significant correlation was observed between the SUV↑, $\overline{SUV}$ and tBF-ScOC values in the overall patient analysis (Table 2; (p=0.69, 0.58)). Similarly, no significant correlation was observed in category of patient(s) divided by tumor location (neither in oropharynx nor in laryngopharynx localities; (p=0.41, 0.62 respectively)). However, a moderate positive but non-significant correlation was observed between the SUV↑ (r=0.37, p=0.11) or the $\overline{SUV}$ (r=0.39, p=0.13) and the tBF-ScOC values in non-advanced T-stages ($T_{1a}/T_{1b}/T_2/T_3$) in the category of patient(s) divided by tumor T-stage. Figure 1 shows that in the advanced T-stage patients, there was a significant negative correlation between both SUVs (SUV↑ and $\overline{SUV}$) and tBF-ScOC values as: for SUV↑, (r=–0.70, $p<0.05$) and for $\overline{SUV}$, (r=–0.73, $p<0.05$). In addition, there was a significant positive correlation between both SUVs (SUV↑ and $\overline{SUV}$) and tBF-ScOC values for the first 2 combinations of subcategories of patient(s) (see "Statistical analysis" section; combination (1) and (2)) (Figures 2, 3), while

Indexed in: [Current Contents/Clinical Medicine] [SCI Expanded] [ISI Alerting System] [ISI Journals Master List] [Index Medicus/MEDLINE] [EMBASE/Excerpta Medica] [Chemical Abstracts/CAS] [Index Copernicus]

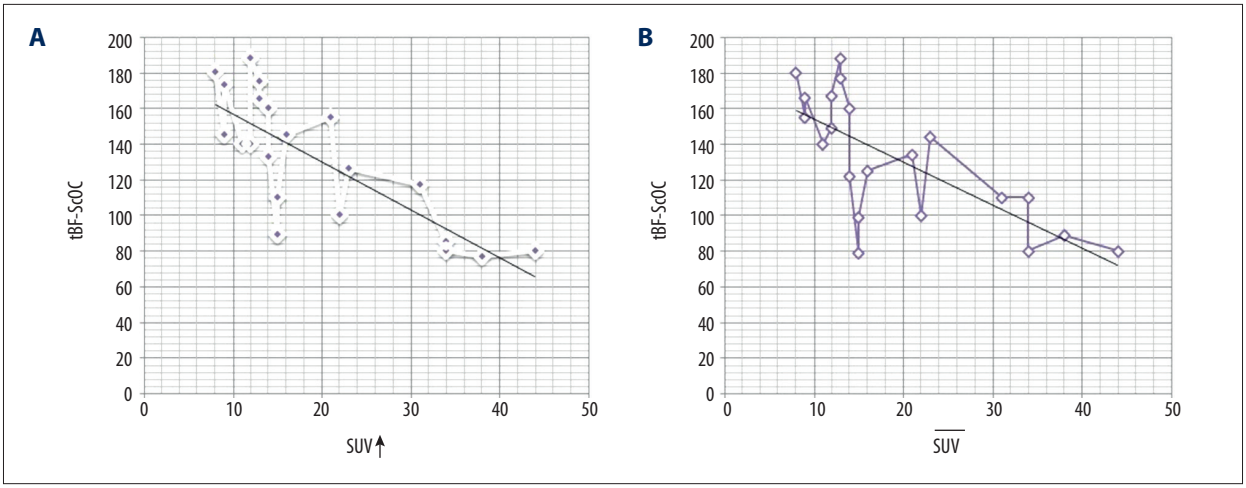

Figure 4. Scatter plot (with straight lines) of the SUV (SUV↑/$\overline{SUV}$) and tBF-ScOC values in the combination of oropharynx locality category patients with advanced T-stage (T_{4a} and T_{4b}) (n=21). There were significant negative correlations (in terms of Pearson's correlation coefficient (r)): (**A**) between SUV↑ and tBF-ScOC values (–0.70 ($p<0.05$)); and (B) between $\overline{SUV}$ and tBF-ScOC values (–0.73 ($p<0.05$)).

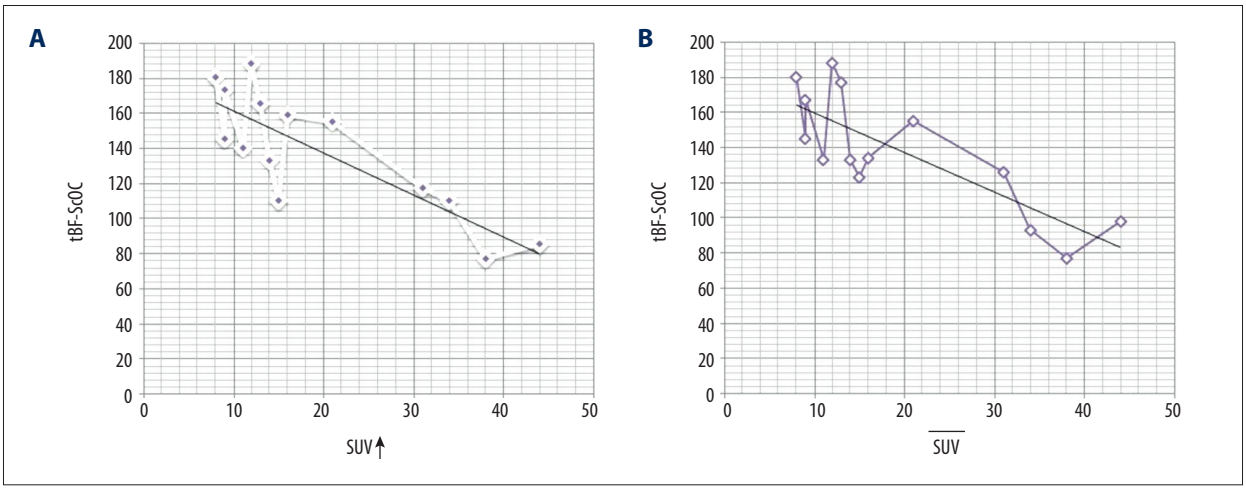

Figure 5. Scatter plot (with straight lines) of the SUV (SUV↑/$\overline{SUV}$) and tBF-ScOC values in the combination of laryngopharynx locality category patients with advanced T-stage (T_{4a} and T_{4b}) (n=14). There were significant negative correlations (in terms of Pearson's correlation coefficient (r)): (**A**) between SUV↑ and tBF-ScOC values (–0.73 ($p<0.05$)); and (**B**) between $\overline{SUV}$ and tBF-ScOC values (–0.75 ($p<0.05$)).

a significant negative correlation was observed for the last 2 combinations of subcategories of patient(s) (see "Statistical analysis" section; combination (3) and (4)) as shown in Figures 4 and 5.

Discussion

Our results show a positive correlation between the non-advanced T-stages of the oropharynx and laryngopharynx localities and SUV↑/$\overline{SUV}$ and tBF-ScOC values. In addition, there was a negative correlation between the advanced T-stage patients for the oropharynx and laryngopharynx localities and SUV↑/$\overline{SUV}$ and tBF-ScOC values. Nevertheless, in the total patient analysis, there was no correlation. A positive correlation between SUV uptake and tumor blood flow values has been reported [24], but the study was very limited in that it had only 2 T_4-staged patients in the total population of 15 patients. However, the study supports our results of positive correlations achieved for non-advanced T-staged patients with both the oropharynx (n=21) and laryngopharynx (n=14) localities between SUV↑/$\overline{SUV}$ and tBF-ScOC values. Angiogenesis and neovascularization take place with the progression of squamous cell carcinoma from an early stage; therefore, the tumor glucose uptake increases in similar fashion. We also observed this well-established correlation in our study.

Indexed in: [Current Contents/Clinical Medicine] [SCI Expanded] [ISI Alerting System] [ISI Journals Master List] [Index Medicus/MEDLINE] [EMBASE/Excerpta Medica] [Chemical Abstracts/CAS] [Index Copernicus]

Interestingly, there is a report [33] showing a negative correlation between SUV and tumor blood flow values in head and neck tumor patients, thus supporting our finding of a negative correlation between SUV↑/$\overline{SUV}$ and tBF-ScOC values in patients with advanced T-stage status, regardless of their primary lesions (Figures 1, 4, 5). However, a previous study [33] found only 9 out of 16 tumors were squamous cell carcinoma. Other limitations in that work [33] were: (a) a negative correlation between the tumor blood flow and SUV values was obtained only in their patient category with large-tumor sizes (>8 cm), and (b) the detailed data of T-stages of the patients were not presented and remained unclear. This might be because the included large-tumor category could only be formed from advanced T-stage patients and this would be quite congruent with our results with respect to the advanced T-stage category. The reason behind this negative correlation is the inclusion of tumors with uncoupling of the SUV (SUV↑/$\overline{SUV}$) and tBF-ScOC uptake, and this uncoupling happens because: (a) the tumor remains aggressive with a high SUV (SUV↑/$\overline{SUV}$) in anaerobic glycolysis; (b) as the tumor grows, it reduces tBF-ScOC and hence angiogenesis cannot maintain an adequate level of blood supply; (c) reduced tBF-ScOC leads to reduced tissue oxygenation (i.e., tumor hypoxia) [33,34]. This reduced tBF-ScOC may lead to a dissimilarity in SUV (SUV↑/$\overline{SUV}$) and tBF-ScOC uptake. This conclusion was clearly identified in our study, in which for several patients we found reduced tBF-ScOC values in comparison to high SUV (SUV↑/$\overline{SUV}$) values. Some studies [22–27] found no correlation between SUV uptake and the tissue blood flow. We suspect that this was because they included both the positive and negative correlations in the overall correlation assessments. Thus, the reason for these different conclusions with respect to the relationship between SUV and tumor blood flow in previous reports is the difference in the T-stages and tumor locations. However, in our study we found that in early non-advanced stage there is increased tBF-ScOC and glucose uptake with ScOC growth, while in the later advanced stage there is a dissimilarity in SUV (SUV↑/$\overline{SUV}$) and tBF-ScOC uptake, which leads to their uncoupling and eventually results in a negative correlation between SUV and tBF-ScOC uptake. Thus, the mechanism of glucose uptake and tBF-ScOC has been established.

Conclusions

We conclude that there is a significant correlation between glucose uptake and tBF in ScOC growth on the basis of tumor locations and tumor T-stages. This establishes the mechanism, which will advance our understanding of the complex tumor behavior in ScOC growth, providing useful information for use in the diagnosis, treatment, and care of ScOC patients.

References:

1. Shimizu M, Mitsudo K, Koike I et al: Prognostic value of 2-[^{18}F]fluoro-2-deoxy-D-glucose positron emission tomography for patients with oral squamous cell carcinoma treated with retrograde superselective intra-arterial chemotherapy and daily concurrent radiotherapy. Oral Surg Oral Med Oral Pathol Oral Radiol, 2016; 121(3): 239–47
2. Wu X, Mastronicola R, Tu Q et al: A rare case of extremely high counts of circulating tumor cells detected in a patient with an oral squamous cell carcinoma. BMC Cancer, 2016; 16: 552
3. Kitajima K, Suenaga Y, Minamikawa T et al: Clinical significance of SUVmax in ^{18}F-FDG PET/CT scan for detecting nodal metastases in patients with oral squamous cell carcinoma. Springerplus, 2015; 4: 718
4. Ido T, Wan CN, Casella V et al: Labeled 2-deoxy-D-glucose analogs. 18F-labeled 2-deoxy-2-fluoro-D-glucose, 2-deoxy-2-fluoro-D-mannose and C-14-2-deoxy-2-fluoro-D-glucose. J Labelled Comp Radiopharm, 1978; 14: 175–82
5. Torizuka T, Tamaki N, Inokuma T et al: Hepatocellular carcinoma with FDG-PET. J Nucl Med, 1995; 36: 1811–17
6. San-Millan I, Brooks GA: Reexamining cancer metabolism: Lactate production for carcinogenesis could be the purpose and explanation of the Warburg effect. Carcinogenesis, 2016 [Epub ahead of print]
7. Miao Y, Zhang LF, Guo R et al: (18)F-FDG PET/CT for monitoring the response of breast cancer to miR-143-based therapeutics by targeting tumor glycolysis. Mol Ther Nucleic Acids, 2016; 5(8): e357
8. Ferlay J, Soerjomataram I, Ervik M et al: Cancer incidence and mortality worldwide: Sources, methods and major patterns in GLOBOCAN 2012. Int J Cancer, 2015; 136: E359–86
9. Hu Y, Hu C, Zhang H et al: How does the number of resected lymph nodes influence TNM staging and prognosis for esophageal carcinoma? Ann Surg Oncol, 2010; 17: 784–90
10. Taghipour M, Sheikhbahaei S, Marashdeh W et al: Use of ^{18}F-flu-deoxyglucose-positron emission tomography/computed tomography for patient management and out-come in oropharyngeal squamous cell carcinoma: a review. JAMA Otolaryngol Head Neck Surg, 2016; 142: 79–85
11. Yokobori Y, Toyoda M, Sakakura K et al: (18)F-FDG uptake on PET correlates with biological potential in early oral squamous cell carcinoma. Acta Otolaryngol, 2015; 135(5): 494–99
12. Pereira KM, Feitosa SG, Lima AT et al: Immunohistochemical evaluation of glucose transporter type 1 in epithelial dysplasia and oral squamous cell carcinoma. Asian Pac J Cancer Prev, 2016; 17(1): 147–51
13. Allal AS, Dulguerov P, Allaoua M et al: Standardized uptake value of 2-[(18)F] fluoro-2-deoxy-D-glucose in predicting outcome in head and neck carcinomas treated by radiotherapy with or without chemotherapy. J Clin Oncol, 2002; 20: 1398–404
14. Davies A, Tan C, Paschalides C et al: FDG-PET maximum standardised uptake value is associated with variation in survival: Analysis of 498 lung cancer patients. Lung Cancer, 2007; 55: 75–78
15. Sasaki R, Komaki R, Macapinlac H et al: [18F]fluorodeoxyglucose uptake by positron emission tomography predicts outcome of non-small-cell lung cancer. J Clin Oncol, 2005; 23: 1136–43
16. Djuric-Stefanovic A, Micev M, Stojanovic-Rundic S et al: Absolute CT perfusion parameter values after the neoadjuvant chemoradiotherapy of the squamous cell esophageal carcinoma correlate with the histopathologic tumorregression grade. Eur J Radiol, 2015; 84(12): 2477–84
17. Srinivasan A, Mohan S, Mukherji SK: Biologic imaging of head and neck cancer: The present and the future. Am J Neuroradiol, 2012; 33: 586–94
18. Ahlgren A, Wirestam R, Lind E et al: A linear mixed perfusion model for tissue partial volume correction of perfusionestimates in dynamic susceptibility contrast MRI: Impact on absolute quantification, repeatability, and agreement with pseudo-continuous arterial spin labeling. Magn Reson Med, 2016 [Epub ahead of print]
19. Han PK, Choi SH, Park SH: Investigation of control scans in pseudo-continuous arterial spin labeling (pCASL): Strategies for improving sensitivity and reliability of pCASL. Magn Reson Med, 2016 [Epub ahead of print]
20. Lyu Y, Liu S, You H et al: Evaluation of recurrent high-grade gliomas treated with bevacizumab: A preliminary report of 3D pseudocontinuous artery spinlabeling. J Magn Reson Imaging, 2016 [Epub ahead of print]

Indexed in: [Current Contents/Clinical Medicine] [SCI Expanded] [ISI Alerting System] [ISI Journals Master List] [Index Medicus/MEDLINE] [EMBASE/Excerpta Medica] [Chemical Abstracts/CAS] [Index Copernicus]

21. Sun L, Liu L, Fu H et al: Association of decreased expression of serum mir-9 with poor prognosis of oral squamous cell carcinoma patients. Med Sci Monit, 2016; 22: 289–94
22. Liao L, Wang J, Ouyang S et al: Expression and clinical significance of microRNA-1246 in human oral squamous cell carcinoma. Med Sci Monit, 2015; 21: 776–81
23. Lei W, Liu Y, Zheng Y et al: MiR-429 Inhibits oral squamous cell carcinoma growth by targeting ZEB1. Med Sci Monit, 2015; 21: 383–89
24. Bisdas S, Spicer K, Rumboldt Z: Whole-tumor perfusion CT parameters and glucose metabolism measurements in head and neck squamous cell carcinomas: A pilot study using combined positron-emission tomography/CT imaging. Am J Neuroradiol, 2008; 29: 1376–81
25. Komar G, Seppanen M, Eskola O et al: 18F-EF5: A new PET tracer for imaging hypoxia in head and neck cancer. J Nucl Med, 2008; 49: 1944–51
26. Veit-Haibach P, Schmid D, Strobel K et al: Combined PET/CT-perfusion in patients with head and neck cancers. Eur Radiol, 2013; 23: 163–73
27. Komar G, Lehtio K, Seppanen M et al: Prognostic value of tumour blood flow, [18F]EF5 and [18F]FDG PET/CT imaging in patients with head and neck cancer treated with radiochemotherapy. Eur J Nucl Med Mol Imaging, 2014; 41: 2042–50
28. Panin VY, Kehren F, Michel C et al: Fully 3-D PET reconstruction with system matrix derived from point source measurements. IEEE Trans Med Imaging, 2006; 25: 907–21
29. Wang Z, Aguirre GK, Rao H et al: Empirical optimization of ASL data analysis using an ASL data processing toolbox: ASLtbx. Magn Reson Imaging, 2008; 26: 261–69
30. Talagala SL, Ye FQ, Ledden PJ et al: Whole-brain 3D perfusion MRI at 3.0 T using CASL with a separate labeling coil. Magn Reson Med, 2004; 52: 131–40
31. van Osch MJ, Teeuwisse WM, van Walderveen MA et al: Can arterial spin labeling detect white matter perfusion signal? Magn Reson Med, 2009; 62: 165–73
32. Fruehwald-Pallamar J, Czerny C, Mayerhoefer ME et al: Functional imaging in head and neck squamous cell carcinoma: Correlation of PET/CT and diffusion-weighted imaging at 3 Tesla. EurJ Nucl Med Mol Imaging, 2011; 38: 1009–19
33. Hirasawa S, Tsushima Y, Takei H et al: Inverse correlation between tumor perfusion and glucose uptake in human head and neck tumors. Acad Radiol, 2007; 14: 312–18
34. Newbold K, Castellano I, Charles-Edwards E et al: An exploratory study into the role of dynamic contrast-enhanced magnetic resonance imaging or perfusion computed tomography for detection of intratumoral hypoxia in head-and-neck cancer. Int J Radiat Oncol Biol Phys, 2009; 74: 29–37

Indexed in: [Current Contents/Clinical Medicine] [SCI Expanded] [ISI Alerting System] [ISI Journals Master List] [Index Medicus/MEDLINE] [EMBASE/Excerpta Medica] [Chemical Abstracts/CAS] [Index Copernicus]